ScanSAR resolution enhancement in bistatic operation

Virginie Kubica, Xavier Neyt

Electrical Engineering Dept., Royal Military Academy, Belgium

Keywords: Bistatic radar, ScanSAR, TOPSAR, resolution enhancement.

Abstract

The ScanSAR mode allows imaging of a swath much wider than range ambiguity limits would normally allow but at the cost of degraded cross-range resolution. This degraded cross-range resolution in monostatic configuration can be enhanced in the case of a bistatic configuration with a receiver close to the imaged area by exploiting the sidelobe emissions of the beams illuminating the adjacent sub-swaths.

In this paper, we will assess the feasibility of enhancing the cross-range resolution in ScanSAR modes of spaceborne transmitters and evaluate the impact on the revisit time. A preliminary analysis of the performance of the method on the novel ScanSAR mode, TOPSAR, is provided.

1 Introduction

To image large swaths at the expense of cross-range resolution, ScanSAR operating satellites, such as RADARSAT-2 [1] and ENVISAT [2], consecutively illuminate several sub-swaths by steering their antenna in elevation.

In monostatic SAR, the 'burst' nature of the ScanSAR signal creates gaps in the synthetic aperture, leading to grating lobes, which if not accounted for using conventional methods [3, 4], severely degrades the radar images.

In opportunistic SAR, i.e. bistatic SAR using emitters of opportunity, the sidelobe radiations of the ScanSAR beams which illuminate the adjacent sub-swaths can be exploited to fill the interburst intervals of the sub-swath which we wish to receive. This will restore the cross-range resolution by removing the grating lobes, provided that the amplitude of the signals transmitted in the sidelobes is sufficient, as is the case for some geometries.

Hence, for satellite passes exhibiting a favourable geometry, the ScanSAR mode can be exploited by an opportunistic SAR radar close to the imaged area to produce enhanced cross-range resolution images. As there are many more passes in the ScanSAR mode than in the Stripmap mode, this results in a decreased revisit time over the area of interest.

This method performs consistently well in ScanSAR mode overpasses for which the remaining interburst intervals are very small. However, the interburst intervals can remain large even for geometrically favourable acquisition such as, for instance, in the Global Monitoring mode of the ENVISAT satellite, which has now unfortunately ceased to transmit. These grating lobes can be controlled by using an appropriate receiving antenna pattern.

A novel type of wide swath imaging mode, TOPSAR (Terrain Observation by Progressive Scans SAR) [5], will be used by the ESA Sentinel-1 SAR instrument and is intended to replace the conventional ScanSAR mode on TerraSAR-X [6]. The method developed in this study can be extended to this new burst-mode SAR.

The paper is organized as follows. Section 2 describes the design of the passive bistatic radar. In Section 3, the cross-range resolution enhancement method is described. This is discussed in detail in Section 4, where a preliminary discussion is given to the analysis of the TOPSAR mode from a bistatic point of view. Finally, Section 5 concludes the paper.

2 Passive SAR system

The passive SAR system considered in this paper consists in an opportunistic spaceborne transmitter operating in ScanSAR mode [3] and a stationary ground-based receiver as illustrated in Fig. 1.

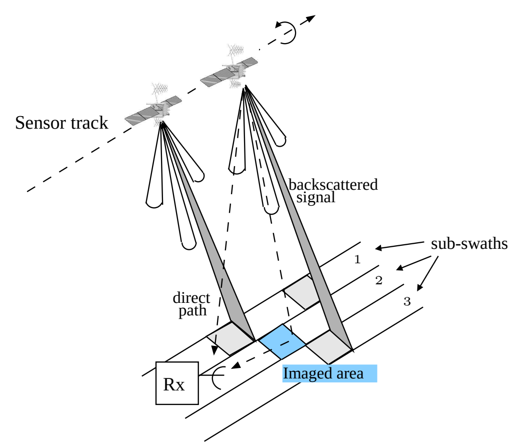

Figure 1: Geometry of the bistatic SAR operating in ScanSAR mode.

Because of this bistatic geometry, the receiver can receive echoes from the sidelobes emissions from the transmitter. The reason for this is twofold: on the one hand the transmit signal is only attenuated by the one-way transmit antenna gain pattern, and on the other hand, for a receiver close to the observed area, the scatterer-receiver distance is much smaller than the scatterer-transmitter distance of the monostatic case yielding a smaller free-space loss in the bistatic case.

2.1 Reception system

The receiving system consists of a classical heterodyne receiver tailored for C-band (ENVISAT, RADARSAT). Figure 2 shows its block diagram which is described in detail in [7]. The received signals are amplified by a cascade of LNAs (Low Noise Amplifier) and analogue down-converted to an intermediate frequency. They are then sampled at 50 MSamples/s using a 16-bit A/D card (AlazarTech ATS660) after an anti-aliasing filter. Finally, they are digitally down-converted to base-band.
Next, signal separation is performed to extract the reference signal (direct-path signal) from the reflected signal.
Finally, an image is synthesized from the separated signals using matched filtering.

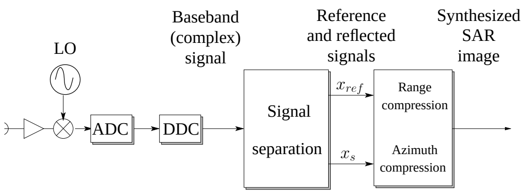

Figure 2: Signal Processing diagram with an analogue (ADC) followed by a digital down-conversion (DDC).

2.2 Transmitter of opportunity

The signals in Fig. 3 result from the Advanced Synthetic Aperture Radar (ASAR) ScanSAR mode transmissions of the ENVISAT satellite, where the transmit beam is steered in elevation to scan different part of the swath along track. In each beam, a burst of several pulses is transmitted. As illustrated in Fig. 3, the bursts are shorter in the Global Monitoring (GM) mode than in the Wide Swath (WS) mode which corresponds to the coarser cross-range resolution stated by the operators for the GM mode.
On Fig. 3 (b) and (d), the bursts corresponding to all different sub-swath are received. Note that the interburst intervals in GM mode remain large even when the receiver/scatterers are illuminated by all five beams.
The amplitude of the bursts is obviously determined by the azimuth antenna diagram but also, for each beam, by the corresponding elevation antenna diagram at the elevation angle at which the receiver/scatterers are located.

3 Passive ScanSAR imaging

In this section, the issues due to the 'burst' nature of the ScanSAR mode and its countermeasure are illustrated using first simulated data and then, real measurements. The study has been performed by using ENVISAT as transmitter of opportunity but can be extended to any other burst-mode SAR satellites.
The Peak-to-SideLobe Ratio (PSLR) is considered to assess the impact of the ScanSAR mode on the image obtained. The PSLR is defined as the ratio of the peak intensity of the most intense sidelobe to the peak intensity in the main-lobe of the Impulse Response Function (IRF) along a one-dimensional profile (in the azimuth direction here).

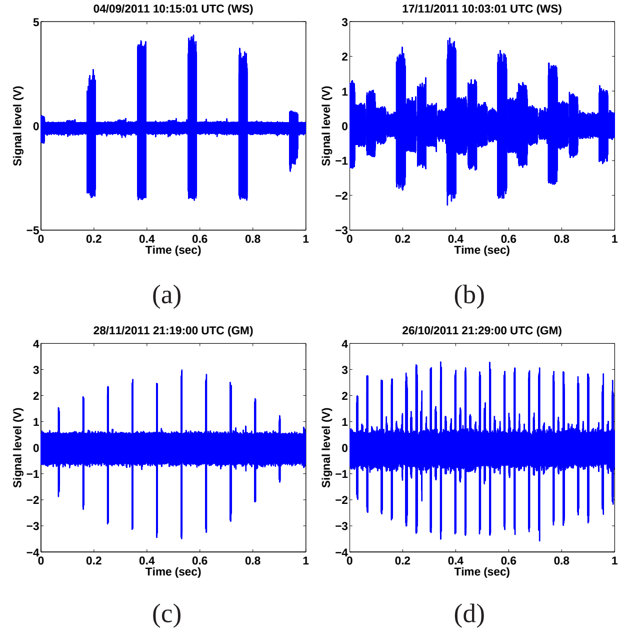

Figure 3: Acquired ENVISAT's signals: (a) and (b) in WS, (c) and (d) in GM modes.

3.1 Signal model

The azimuth amplitude modulation can be modeled by

$$y(t) = w(t)x(t) + n(t) \tag{1}$$

where $y(t)$ is the ScanSAR azimuth amplitude modulated signal with t the slow-time, $x(t)$ the received signal (pulses) assuming a constant amplitude (independent of the ScanSAR beam), $w(t)$ an amplitude modulation function representing the transmitter antenna gain at the elevation of the receiver/imaged area and which varies with each ScanSAR beam and $n(t)$ the noise (thermal noise and eventual interference from scatterers located in the main beam i.e. at another range than the range of interest). $x(t)$ and $n(t)$ are further assumed to be uncorrelated.
The internal amplitude structure of the window $w(t)$ represents the relative amplitude of the different beams in elevation as seen by the receiver/scatterers on the ground. This azimuthal amplitude modulation will vary with the position of the receiver/scatterer in the global swath.

3.2 Bistatic sidelobes imaging

For illustrative purpose, a scenario with a point scatterer in presence of noise (SNR of $-10dB$) is considered. This scatterer is located far away from the range sidelobes of the direct-path signal in order to avoid direct path interferences on the scatterer impulse response.
For illustrative purpose, two extreme cases have been envisaged. First, a single-beam ScanSAR mode, as would be obtained for a receiver/scatterer at the very edge of the wide swath illuminated by one single-beam, would result

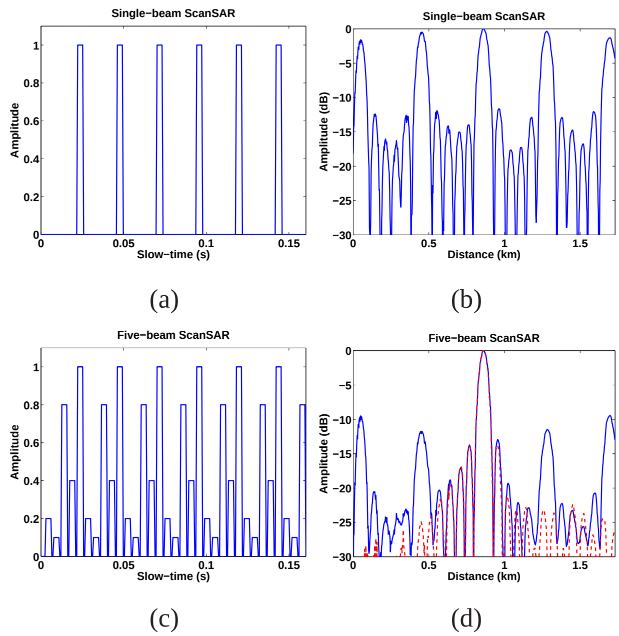

Figure 4: On the left, window functions $w(t)$ of the two extreme ScanSAR modes, and on the right, cuts along the scatterer's isorange using the matched filter (solid line). The graph (below right) shows the IRF after amplitude compensation (dashed line).

in a pulse-train window modulation as illustrated in Fig. 4 (a). The spectrum of that window predicts the azimuthal impulse response[1] in the case of matched filter processing and as is well known [3, 4], azimuth grating lobes appear in the IRF. This is illustrated in Fig. 4 (b), with a PSLR of about -0.1dB.

When the receiver/scatterer is ideally situated, i.e. at the centre of the global swath, reception of signals from all five elevation beams is possible but each with a different amplitude according to the elevation antenna diagram of the considered beam as shown in Fig. 4 (c). The *gaps* present in the single-beam ScanSAR mode will then be filled, hence the name gap-filling method.

Processing of the data *as such* using matched filtering leads to a reduction of the amplitude of the grating lobes as shown in Fig. 4 (d) (solid line) with a PSLR of -9.7dB improved with respect to the PSLR of a single-beam ScanSAR. That demonstrates that gap-filling is a step in the right direction to approach the Stripmap performance.

3.3 Amplitude compensation method

To further reduce the grating lobes leading to ambiguities in the SAR image, an amplitude compensation method is proposed. The aim of the method is to estimate $x(t)$ given the measurement $y(t)$. The estimation of the unknown signal, $x(t)$, can be done by designing the window $h(t)$ to minimize the Mean Square Error $E[|x(t) - h(t)y(t)|^2]$ between the unknown true signal $x(t)$ and its estimate $h(t)y(t)$,

[1] Only when the PRI is constant in each ScanSAR beam, what is assumed here for convenience. In reality, it varies with the antenna elevation angle of the beam to avoid range ambiguities [8].

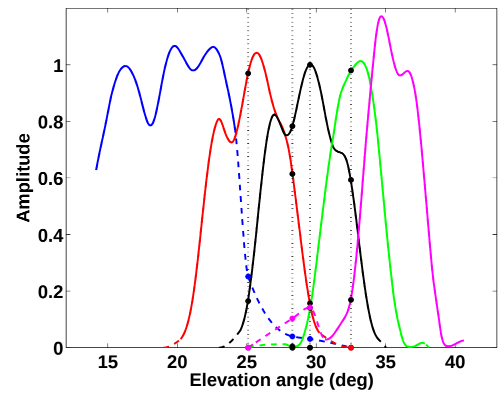

Figure 5: Extrapolated antenna elevation diagrams of the 5 beams of the ASAR antenna. The coloured dots on the dashed line denote our measurements and the black dots on the solid line denote the values obtained from sampling antenna patterns provided by ESA.

leading to

$$h_{opt}(t) = \frac{w(t)}{|w(t)|^2 + \frac{\sigma^2}{E[|x(t)|^2]}}, \qquad (2)$$

σ^2 being the variance of the noise.

For a favourable SNR of $-10dB$, it should be remarked that the residual grating lobes due to the ScanSAR data totally disappear when $h_{opt}(t)$ is applied as illustrated in Fig. 4 (d). That will be the case if the amplitudes of the received pulses in all the five beams are sufficient i.e. for sufficient SNR.

3.4 Performance prediction

The beam-to-beam amplitude difference is dictated by the position of the receiver in the swath covered by the transmitter. Note that the range from the receiver to the area being imaged is short relative to the swath width and hence, the same beam-to-beam amplitude difference can be assumed. The position of the receiver/imaged area in the swath are defined by the antenna elevation angle, i.e., the angle scatterer-transmitter-nadir. Therefore, this key parameter can predict whether or not the planned ScanSAR pass is suitable for amplitude-compensated cross-range resolution-enhanced SAR imaging. The bistatic geometry is calculated using the satellite position obtained with the help of an SGP4 orbit propagator and orbital information from the two line elements of the considered satellite.

For performance prediction, knowledge of the amplitude of the sidelobes of the elevation diagram is of utmost importance. As the European Space Agency (ESA) only provides the elevation antenna diagrams of the ASAR antenna for 5° around the beam centre, data acquired over six months by the aforementioned bistatic system were used to complement the elevation diagrams at other angles.

Figure 5 depicts the ESA calibrated amplitude elevation diagrams of the five beams of ASAR used in ScanSAR mode (solid lines) and the extrapolation (dashed lines) based on our measurements.

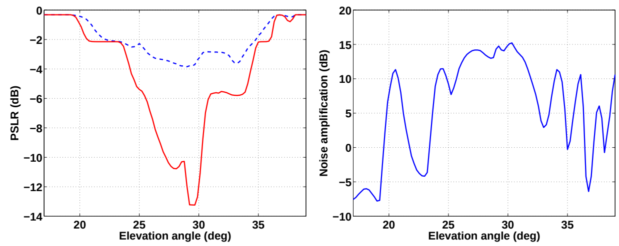

(a) (b)

Figure 6: (a) Calculated PSLR for different antenna elevation angles without compensation (dashed line) and with compensation (solid line) and (b) calculated relative noise energy (w.r.t. Stripmap mode) amplification of the compensation method.

To illustrate the influence of the antenna elevation angle, a scenario similar to that of Section 3.2 with a more realistic SNR of $-40dB$ is considered where different satellite passes over $15° \leq \theta_{el} \leq 40°$ are simulated. Then, the PSLRs of the IRF obtained with the conventional matched filter with and without compensation are computed.

Figure 6 (a) reveals that the PSLR of the matched filter with compensation is by far better than without, at least for receivers/scatterer located in the elevation angle range $[27° - 32°]$. However, for a range of small values of $w(t)$, i.e. when one or several beams are barely present (in low SNR areas), $h_{opt}(t)$ strives to find a reasonable balance between, on the one hand, compensation of the weak signals and, on the other hand, amplification of the noise. Figure 6 (b) illustrates the noise amplification effect of $h_{opt}(t)$ for a SNR of $-40dB$: although the grating lobes are reduced, the noise is amplified by up to $15dB$. Hence, the amplitude compensation method applied on geometrically favourable ScanSAR mode passes can recover the cross-range resolution of the Stripmap mode at the expense of an amplification of the noise. In reality, the SNR can not be estimated since the echoed signal $x(t)$ is unknown and hence, a reasonable value is considered. By underestimated the SNR, the amplification of the noise is reduced while the grating lobes are less reduced.

3.5 Result on real measurements

On the 16^{th} of March 2012, the receiver, located in Brussels, was in the centre of the swath of the ASAR instrument of ENVISAT operating in WS mode. Figure 7 illustrates the five-beam RF signal acquired during its overpass. To illustrate the performance of the amplitude compensation method, a point-like target in the image is analyzed.

Consider first the processing of one beam of the ScanSAR acquisition. The expected grating lobes in azimuth along the isorange appears as shown on Fig. 8 (a). After the multi-beam processing, a reduction of the grating lobes below the noise level occurs (Fig. 8 (b)). If the amplitude compensation method is applied with an optimistic value of SNR, the signal as well as the underestimated noise will be compensated which results in an amplification of the noise as illustrated in Fig. 8 (c). For an overestimation of the noise

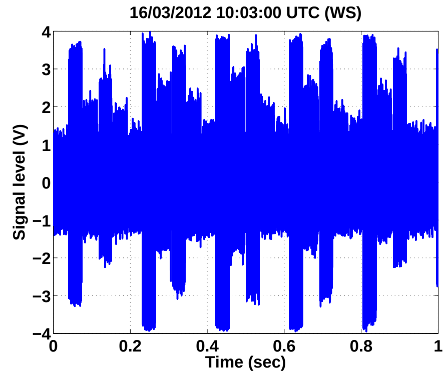

Figure 7: Signal acquired during an overpass of ENVISAT operating in WS mode.

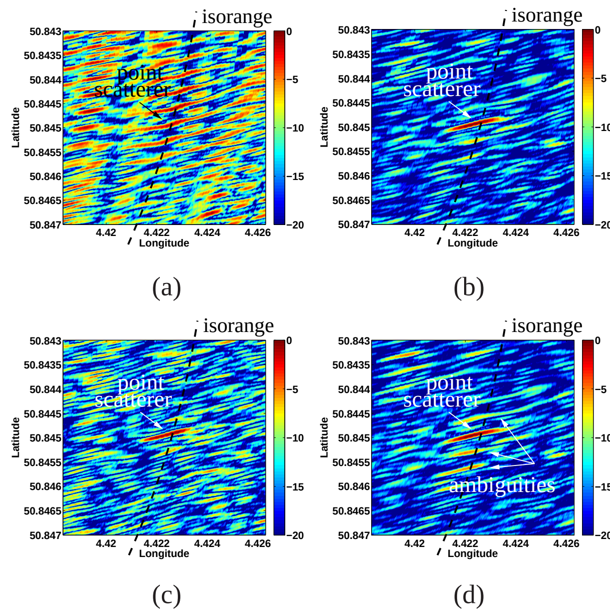

Figure 8: Zoom on a point scatterer in the georeferenced SAR image (a) for a single-beam processing, (b) for a multi-beam processing, (c) and (d) for a multi-beam processing with respectively an optimistic and a pessimistic amplitude compensation method.

(pessimistic value of SNR), the amplification of the noise is low while the grating lobes are less reduced and reappear as shown on Fig. 8 (d).

4 Discussions

4.1 Impact of interburst interval

The performance of the gap-filling method depends on the remaining interburst interval. In WS mode, the remaining gaps are so small that the resulting grating lobes, which are widely separated, will not degrade SAR imaging as they will not be within the bistatic footprint. However, even for a five-beam reception configuration, the GM mode still presents large gaps in the coherent phase history data. This results in closer grating lobes which still impair SAR imaging.

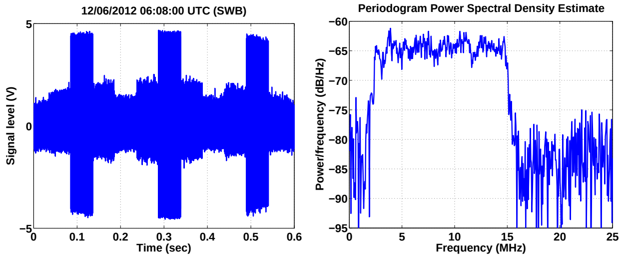

(a) (b)

Figure 9: (a) Three cycles of a RADARSAT-2 signal in ScanSAR Wide mode B and (b) its power spectral density estimation.

The obvious solution to this issue is to limit the field of view (FOV) of the receiver by using a directive receiving antenna which is easily done in a bistatic configuration. Note that improving the cross-range resolution of a ScanSAR operating transmitter is only meaningful if the range resolution is of the same order of magnitude which was not the case for the GM mode of ENVISAT.

Figure 9 (a) illustrates the four-beam RF signal received from RADARSAT-2 on the 12^{th} of June 2012 in the ScanSAR Wide mode SWB. The measured bandwidth is constant from beam-to-beam and is equal to $11,56MHz$ which is of the same order of magnitude as the bandwidth of the WS mode of ENVISAT (Fig. 9 (b)). Zero interburst interval in the SWB mode of RADARSAT-2 was noticed suggesting a better performance of the amplitude compensation method.

4.2 Impact on revisit time

During a period of six months (June-Dec 2011), about 25 ENVISAT passes were recorded over Brussels. 2 were in Stripmap Mode while the other 23 were in ScanSAR mode (12 in GM and 11 in WS). 7 of the 11 WS passes were in the favourable elevation angle range $[27° - 32°]$. This means that 64% had a PSLR low enough to guarantee an acceptable grating lobes reduction at the expense of a higher noise level. This increases the revisit time with a factor of 5. In GM mode, half of the overpasses were geometrically favourable, leading to a total increase of the revisit time by a factor of 7 if a directive receiving antenna is used.

4.3 TOPSAR preliminary analysis

While in the ScanSAR mode the antenna is steered only in the range direction, in TOPSAR mode, the antenna is steered in both azimuth and range as depicted in Fig. 10. The TOPSAR mode consists in rotating the antenna throughout the transmission from backward to forward at a constant rotation speed, opposite to the spotlight case [9]. This results in the shrinking of the azimuth antenna pattern (AAP), i.e. a worsening of the cross-range resolution compared to ScanSAR but in favor of a reduction of the scalloping effect [10] since each point is illuminated by the same AAP.

Figure 10 depicts the scan pattern of the transmit antenna operating in TOPSAR mode with two sub-swaths. The scan pattern is characterized by a very long burst time, T_B, in order to be able to illuminate each point with the main lobe.

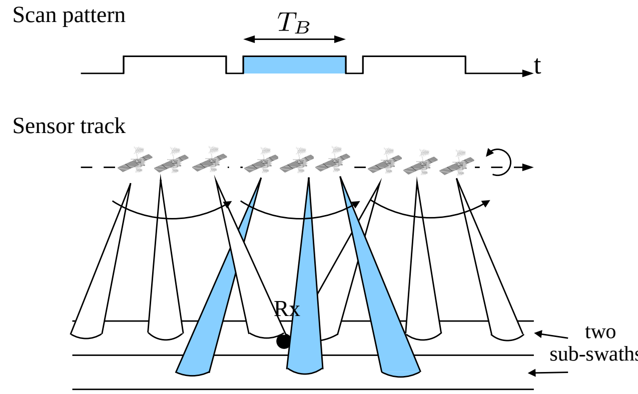

Figure 10: TOPSAR acquisition geometry.

For a receiver located in sub-swath 1, the likely azimuth data from a TOPSAR pass is illustrated in Fig. 11. The area imaged by the receiver is first illuminated by the azimuth sidelobes of the transmitter which, at the end of the burst, steers its azimuth main lobe in the direction of the receiver and the imaged area. Then, after switching the antenna elevation beam to the second range sub-swath, the transmitter illuminates the area of interest via its elevation sidelobes.

For each elevation angle of the transmit antenna, the same AAP can be recognized but scaled by the elevation gain corresponding to the elevation angle at which the receiver/observed area are located. Note that the main lobe experiences a shift as a function of the along-track position of the receiver.

The contraction of the AAP is determined by the antenna steering velocity in azimuth. If the main lobe of the shrunk AAP is small, the azimuth data profile suggests a similar case to that of the GM mode of ENVISAT where the long interburst intervals are represented in TOPSAR mode by many low azimuth sidelobes.

As a conclusion, the antenna steering law of the TOPSAR mode will determine the performance of the beam-to-beam amplitude differences compensation method.

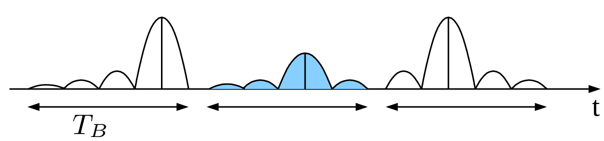

Figure 11: Azimuth data acquired by a ground-based receiver located in sub-swath 1.

5 Conclusions

In this paper, we have illustrated that, under favourable geometrical conditions, a bistatic receiver is able to reduce the grating lobes inherent to the ScanSAR modes by filling the interburst intervals with the sidelobe emissions of the adjacent beams.

Besides, these residual grating lobes can be suppressed by applying a beam-to-beam amplitude differences compensation method that will restore the cross-range resolution of the Stripmap mode at the expense of an amplification of the noise. This significantly decreases the revisit time of high cross-range resolution images.

Furthermore, in ScanSAR modes having large interburst intervals such as GM of ENVISAT and using a directive receiving antenna, the amplitude-compensated cross-range resolution-enhanced method is meaningful if the range resolution/bandwidth is increased. One possible application would be the monitoring of structures (such as dam, building, quarry,...) at short distance of the receiver by using for instance interferometry [11].

Finally, a preliminary analysis of the TOPSAR mode suggests that the performance of the method developed in this paper depends on the azimuth steering parameter.

References

[1] R. Raney, A. Luscombe, E. Langham, and S. Ahmed, "RADARSAT," *Proceedings of the IEEE*, vol. 79, pp. 839–849, June 1991.

[2] Y.-L. Desnos, C. Buck, J. Guijarro, J.-L. Suchail, R. Torres, and E. Attema, "{ASAR}-{ENVISAT}'s Advanced Synthetic Aperture Radar," *ESA bulletin*, pp. 91–100, May 2000.

[3] R. Bamler and M. Eineder, "ScanSAR processing using standard high precision SAR algorithms," *IEEE Transactions on Geoscience and Remote Sensing*, vol. 34, pp. 212–218, Jan. 1996.

[4] J. Holzner and R. Bamler, "Burst-mode and ScanSAR interferometry," *IEEE Transactions on Geoscience and Remote Sensing*, vol. 40, no. 9, pp. 1917–1934, 2002.

[5] F. De Zan and A. Monti Guarnieri, "TOPSAR: Terrain Observation by Progressive Scans," *IEEE Transactions on Geoscience and Remote Sensing*, vol. 44, no. 9, pp. 2352–2360, 2006.

[6] A. Meta, P. Prats, U. Steinbrecher, J. Mittermayer, and S. Rolf, "TerraSAR-X TOPSAR and ScanSAR comparison," in *EUSAR Conference*, (Friedrichshafen, Germany), pp. 277–278, 2008.

[7] E. Cristofani, V. Kubica, and X. Neyt, "A multibeam opportunistic SAR system," in *IEEE Radar Conference*, (Kansas City, MI), May 2011.

[8] R. Moore, J. Claassen, and Y. Lin, "Scanning Spaceborne Synthetic Aperture Radar with Integrated Radiometer," *IEEE Transactions on Aerospace and Electronic Systems*, vol. 17, pp. 410–421, May 1981.

[9] D. D'Aria, D. Giudici, F. De Zan, A. M. Guarnieri, and F. Rocca, "Burst-mode SAR's for wide-swath surveys," *Canadian Journal of Remote Sensing*, vol. 33, pp. 27–38, 2007.

[10] F. De Zan, A. Monti Guarnieri, and F. Rocca, "Advances in SAR interferometry for Sentinel-1 with TOPS," in *IEEE Radar Conference*, pp. 1–6, May 2008.

[11] J. Sanz-Marcos, P. Lopez-Decker, J. J. Mallorqui, A. Aguasca, and P. Prats, "{SABRINA}: A {SAR} Bistatic Receiver for Interferometric Applications," *IEEE Geoscience and Remote Sensing Letters*, vol. 4, pp. 307–311, Apr. 2007.